Journal of Materials Chemistry A

Polymer non-fullerene solar cells of vastly different efficiencies for minor side-chain modification: Impact of charge transfer, carrier lifetime, morphology and mobility

Journal:	*Journal of Materials Chemistry A*
Manuscript ID	TA-ART-02-2017-001746.R3
Article Type:	Paper
Date Submitted by the Author:	04-Jun-2018
Complete List of Authors:	Awartani, Omar ; North Carolina State University, Physics Gautam, Bhoj; North Carolina State University, Physics Zhao, Wenchao; Institute of Chemistry, Chinese Academy of Sciences Younts, Robert; North Carolina State University, Physics Hou, Jianhui ; Institute of Chemistry, Chinese Academy of Sciences, Gundogdu, Kenan; NC State University , Physics Department Ade, Harald; North Carolina State University, Physics

Polymer non-fullerene solar cells of vastly different efficiencies for minor side-chain modification: Impact of charge transfer, carrier lifetime, morphology and mobility

Omar M. Awartani,[a*] Bhoj Gautam,[a, c*] Wenchao Zhao,[b*] Robert Younts[a], Jianhui Hou,[b] Kenan Gundogdu[a] and Harald Ade,[a,+]

The performance of the highly efficient PBDB-T ITIC system with 11.25% power conversion efficiency is degraded significantly to 4.35% when ITIC is blended with a version of PBDB, dubbed PBDB-O, which has only a minor side-chain modification. We explored the reasons for this difference and investigated the impact of morphology, molecular packing and mobility on carrier lifetime and performance. We employed transient absorption spectroscopy to investigate the hole and electron carrier dynamics in each of the blends and observe significant differences in geminate recombination. In order to understand the influence of morphology and mobility on the carrier dynamics and recombination, we utilized grazing incident wide-angle x-ray scattering (GIWAXS), resonant soft x-ray scattering (RSoXS) and diode mobility measurements. Our results indicate that the difference in performance is difficult to explain with the small differences observed in morphology and packing, and seems to be dominated by the changes in intrinsic mobility that the side-chain modification engenders, which impact both charge creation and extraction. The results highlight the difficulties of predicting the impact of synthetic structural modifications on performance and on a specific device-relevant parameter.

[a] *Department of Physics and Organic and Carbon Electronics Laboratory (ORACEL), North Carolina State University, Raleigh, NC 27695, USA. E-mail: Kgundog@ncsu.edu, hwade@ncsu.edu*
[b] *State Key Laboratory of Polymer Physics and Chemistry, Beijing National Laboratory of Molecular Sciences, Institute of Chemistry, Chinese Academy of Sciences, Beijing 100190, P. R. China, +Email: hjhzlz@iccas.ac.cn*
[c] *Department of Chemistry and Physics, Fayetteville State University, Fayetteville, NC 28301, USA.*
** These authors have contributed equally to this work.*
† Electronic Supplementary Information (ESI) available: [details of any supplementary information available should be included here]. See DOI: 10.1039/x0xx00000x

1. Introduction

Non-fullerene small molecule acceptors (NF-SMAs) are emerging as a very promising alternative to fullerenes, as these materials offer several advantages; namely high extinction coefficient,[1] stronger aggregation,[2] highly tunable molecular energy levels[3,4,5], and low reorganization energies associated with lower voltage losses.[6,7,8] In addition to reduced voltage loss, NF-SMAs have potentially higher photocurrent generation as they can synergistically cover, with the donor, a larger spectral range and have high optical absorption. Efficient electron and hole transfer in polymer:NF-SMAs OPVs provides a greater potential in achieving high photocurrents relative to fullerene based OPVs [1,9,10] Another critical factor in optimizing material design is the energy difference between the interfacial (CT) states and the bulk excitonic states in both donor and acceptor. It provides the driving force for efficient charge generation. This driving force is potentially controllable by the delicate alignment of the energy level offsets between the donor and the acceptor materials in NF-SMAs. Furthermore, it is well known that different chemical structures can create a range of D/A docking configuration[11] and vastly different morphologies that can greatly impact device performance.[12,13] It is thus often difficult to predict the impact of a molecular change on specific parameters out of all the factors that impact performance, even though such predictability would be highly desirable.

In a bulk heterojunction, photophysical phenomena such as charge carrier generation, transport and lifetime can be influenced by several different morphological features including docking,[11] miscibility,[14,15] molecular orientation at or relative to the donor/acceptor interface,[12,16,17] domain size and average purity.[18,19] Additionally, charge mobility plays a major role.[20,21,22] Given that the side-chain modifications in the current study are small and side chains remain attached to the same backbone moiety, we presume that differences in docking play a minor role. In contrast, previous work showed that even small side differences can lead to large morphological differences due to changes in aggregation and solublity,[23,24,25] and a detailed delineation of the films' morphological characteristics is needed along with the impact in charge creation and mobility.

Here, we investigate the various factors controlling performance including the underlying photoexcitation processes of two BDD-based donor polymers with slightly different side-chains, that when blended with ITIC yield drastically different performances of 4.3% and 11.2%. The two donor polymers utilized are PBDTBDD-O (poly{1-(5-(4,8-bis((2-ethylhexyl)oxy)-6-methylbenzo[1,2-b:4,5-b']dithiophen-2-yl)thiophen-2-yl)-5,7-bis(2-ethylhexyl)-3-(5-methylthiophen-2-yl)benzo[1,2-c:4,5-c']dithiophene-4,8-dione}) abbreviated as PBDB-O, and PBDTBDD-T (poly[(2,6-(4,8-bis(5-(2-ethylhexyl)thiophen-2-yl)-benzo[1,2-b:4,5-b']dithiophene))-alt-(5,5-(1',3'-di-2-thienyl-5',7'-bis(2-ethylhexyl)benzo[1',2'-c:4',5'-c']dithiophene-4,8-

dione))]) abbreviated as PBDB-T. These two polymers are chemically similar with a slight difference in their side chains, i.e. PBDB-O has an alkoxyl group whereas PBDB-T has an alkylthienyl group instead.[26] These polymers have been previously investigated but without a focus on the underlying optoelectronic processes in devices with NF-SMAs. Morphological and device characterization of these exceptional polymer donors focused on blends with fullerene[26] and n-type polymer[24] as acceptors. Here, each of the polymers is blended with the same NF-SMAs named ITIC (3,9-bis(2-methylene-(3-(1,1-dicyanomethylene)-indanone))-5,5,11,11-tetrakis(4-hexylphenyl)-dithieno[2,3-d:2',3'-d']-s-indaceno[1,2-b:5,6-b']). The small structural change should eliminate major changes in docking configurations as well as differences in energetic offsets as significant variables. We thus investigate the blends with TAS to measure charge creation characteristics, use R-SoXS and GI-WAXS for morphology characterization, and diode measurement for mobility determination. Significant differences are observed in geminate recombination and mobility, but not in packing, texture and morphology.

2. Experimental

2.1 Materials/synthesis: Both PBDB-O and PBDB-T were synthesized according to methods discussed in previous work.[26] PBDB-O Mn=25.3 kg/mol; PDI=2.24; PBDB-T Mn=16.0 kg/mol, PDI=3.25. ITIC was purchased from Solarmer Materials (Beijing) Inc, China. ZnO solution was also cast using previously reported procedures.[2] All other materials were commercially available and were unaltered before using.

2.2 Device Fabrication: The devices were fabricated with an inverted structure of ITO/ZnO/Polymer:ITIC/MoO_3/Al. The ZnO layer was spin-coated on top of a pre-cleaned, UV-Ozone-treated ITO substrate, and then annealed at 200 ^oC for 60 minutes. Subsequently**,** PBDB-O:ITIC (1:1 weight ratio) and PBDB-T:ITIC (1:1 weight ratio) in a 20 mg ml^{-1} chlorobenzene:DIO (99.5:0.5 volume ratio) solution was spin-coated at 2500 RPM for 60 s to obtain a film thickness of approximately 100 nm, respectively. The film thickness data were obtained via a surface profilometer (Dektak XT, Bruker). To control the morphology of the blend film, the active layers were annealed at 160 ^oC for 30 minutes. The details of annealing condition could be found in recent work. [2] Then, the device fabrication was completed by thermally evaporating 10 nm thick MoO_3 and 100 nm thick aluminium under vacuum at a pressure of 3×10^{-4} Pa. The effective area of each device is 4 mm^2 defined by a metal mask.

2.3 Device Measurement: The *J-V* curves of the devices were measured under AM1.5G illumination at 100 mW cm^{-2} using an AAA solar simulator (XES-70S1, SAN-EI Electric Co., Ltd) calibrated with a standard photovoltaic cell equipped with a KG5 filter (certificated by the National Institute of Metrology) and a Keithley 2400 source-measure unit. The EQE data were obtained using a solar cell spectral response measurement system (QE-R3011, Enli Technology Co. Ltd). The carrier mobility of the PBDB-O:ITIC and PBDB-T:ITIC blend films was calculated from *J-V* curves obtained under dark condition with the hole-only and electron-only device structure of ITO/PEDOT:PSS/BHJ/Au and ITO/ZnO/BHJ/Al, respectively. Mott-Gurney law was used for the data fitting of mobilities. The series resistance, built-in voltage and field effect were taken into account. The electron mobility of ITIC was obtained from the literature.[27]

2.4 Morphology Characterization: Grazing Incidence Wide Angle Scattering (GIWAXS) and Resonant Soft X-Ray scattering (RSoXS) measurement were performed at beamlines 7.3.3,[28] and beamline 11.0.1.2,[29] respectively, at the Advanced Light Source (ALS) in Lawrence Berkeley National Lab, Berkeley, CA. For GIWAXS measurements, the samples were measured in a Helium environment to minimize air scattering using 10 keV energy X-rays. The scattered X-rays were detected using a Dectric Pilatus 2M photon counting detector.

2.5 Transient Absorption Spectroscopy: Transient absorption data were collected using a setup that consists of a spectrometer (Ultrafast Helios system) and an amplified Ti:Sapphire laser. The output of the amplified Ti:Saphhire laser provides 800 nm fundamental pulses at 1 kHz repetition rate that were split into two optical beams to generate pump and probe pulses. One fundamental beam was used to generate a pump beam using an optical parametric amplifier (OPA) system (Coherent Opera Solo). A white-light NIR probe was generated by focusing the other fundamental beam onto a flint glass. The pump and probe beams were focused on sample and the probe light was collected by a charge-coupled device (CCD) device. The spectral detection region is from 0.8 eV to 2.6 eV. The thin film samples were encapsulated before the measurement using UV curable glue. The instrument response function (IRF) was ~100 fs FWHM. The samples were excited with excitation energy of 1.77 eV (700 nm) for acceptor excitation and 2.38 eV (520 nm) for donor excitation.

3. Results and discussion

The device structure, chemical structures, optical absorption, J-V and EQE characteristics of the two blends are presented in **Figure 1a-d**. The device characteristics, summarized in **Table 1**, indicate that the drastic difference in PCE is mainly due to a 42% decrease in fill factor and 29% decrease in J_{sc} in the PBDB-O:ITIC device in comparison to the PBDB-T:ITIC. The degradation in the V_{oc} of the PBDB-O:ITIC is only ~6%. The small change in V_{oc} indicates that charge transfer (CT) state energies of the two donor materials are likely similar. Additional measurements such as sensitive external quantum efficiency (EQE) and CT electroluminescence are required to accurately determine the CT state energies and their role in determining the Voc. The slight loss in V_{oc} for PBDB-O:ITIC actually indicates that the driving force for charge separation is slightly larger in PBDB-O:ITIC than in PBDB-T:ITIC, and thus likely an irrelevant factor for the reduced performance. Given the drastic differences in performance and that the energetics of the charge separation is an unlikely source of these differences, the investigation of the subtle differences in driving force are outside the scope of this paper. We conclude and assume below that the driving force for charge creation is comparable in the two blends and that the differences observed are due to the other factors investigated here. The nearly identical absorbance spectra for the two blend films (see **Figure S1**, and **Figure 1b**) makes the spectral coverage a non-contributing factor to the drastic difference in device performance.

We will generally discuss the relevant factors in the order that they occur in the devices, i.e. photon absorption/exciton creation, exciton quenching/charge transfer state creation, free charge generation, recombination, and mobility/extraction. The discussion of the impact of morphology and molecular packing is interspersed just prior to extraction in order to discuss the exciton and charge dynamics in the context of morphological parameters.

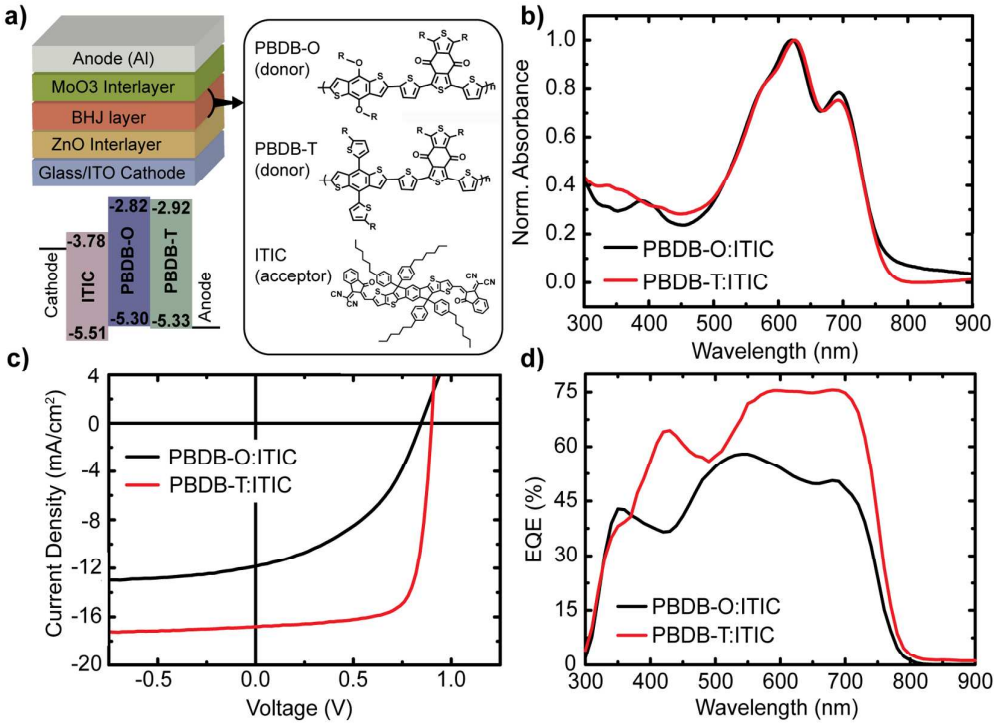

Figure 1. a) Organic solar cell architecture: ITO/ZnO/BHJ/MoO3/Al, chemical structures of the donor polymers and non-fullerene acceptor (ITIC) with corresponding HOMO-LUMO energy levels. b) Normalized UV-Vis absorbance for blend films (absorbance of neat films is provided in **Figure S1**), c) J-V curves d) EQE for PBDB-O:ITIC and PBDB-T:ITIC devices.

Table 1: Device performance parameters for PBDB-O:ITIC and PBDB-T:ITIC solar cells.

Device	V_{oc} (V)	J_{sc} (mA/cm^2)	FF	PCE (%)
PBDB-O:ITIC	0.846	11.86	0.433	4.35
PBDB-T:ITIC	0.899	16.80	0.742	11.21

We investigated the charge separation dynamics and the potential carrier loss due to carrier recombination[7,8,31,32,33] using femtosecond transient absorption spectroscopy (TAS) in the two blend systems. Importantly, unlike in fullerene systems where the hole dynamics can be more or less neglected and is rarely studied, we monitor electron and hole dynamics as both materials contribute substantially to optical absorption and J_{sc}[1] **Figures 2a,b** show the transient absorption spectra in the IR region after the blend samples are excited using pump pulses tuned to 2.38 eV (520 nm), which predominantly create excitons in the donor polymer. The transient absorption spectra of neat polymer films with 2.38 eV excitation are also provided in **Figure S2.** The near IR spectra of both blends exhibit two absorption features at ~1.07 eV and ~1.27 eV. These two peaks correspond to the excited state absorption of the polymer excitons and polarons, respectively. This assignment is consistent with the earlier results of TAS on polymer blends.[8,34,35] To isolate the contributions of the donor singlet excitons and polarons, we used multivariate curve resolution alternating least square analysis[36,37] (MCR-ALS) and deconvoluted the spectra. MCR-ALS is a common tool in spectroscopy to find the associated component spectra and dynamics.[36] A matrix incorporating the dynamics of the excited-state species and another matrix including the spectral bands of the excited-state species were used to recreate the TA spectrum as a function of time. This way we were able to remove the interspecies dependence on spectral bands. The component spectra obtained from MCR-ALS are shown in **Figure S3**, **Figure 2c and 2d** show the comparison of the exciton dynamics of the blend films and neat polymers monitored at the deconvoluted exciton peak centered at ~1.07 eV. The neat polymer exciton dynamics is used as a reference that allows estimating the polymer exciton lifetime. Exciton decay of neat and blended films were fitted with double exponential functions. The weighted exciton lifetime in the neat PBDB-O film is 22 ps whereas it is 21 ps when blended with ITIC (see **Figure 2c**). We also analyzed the prompt charge generation in the ultrafast time scales (<500 fs), and found that negligible amount of polarons generated promptly in PBDB-O blend. In contrast, the excitons in the PBDB-T:ITIC blend decay with a average lifetime of 8 ps, which is substantially shorter compared to the 36 ps lifetime in the neat PBDB-T polymer (**Figure 2d**). These results are summarized in **Table 2**. In addition analysis of the polaron population dynamics indicates that 35% of the excitons charge separate promptly generating polarons. The substantial reduction of the exciton lifetime in the PBDB-T blend suggests efficient creation of charge transfer states, whereas in PBDB-O blend exciton splitting/charge transfer is a problem and hence eventual charge

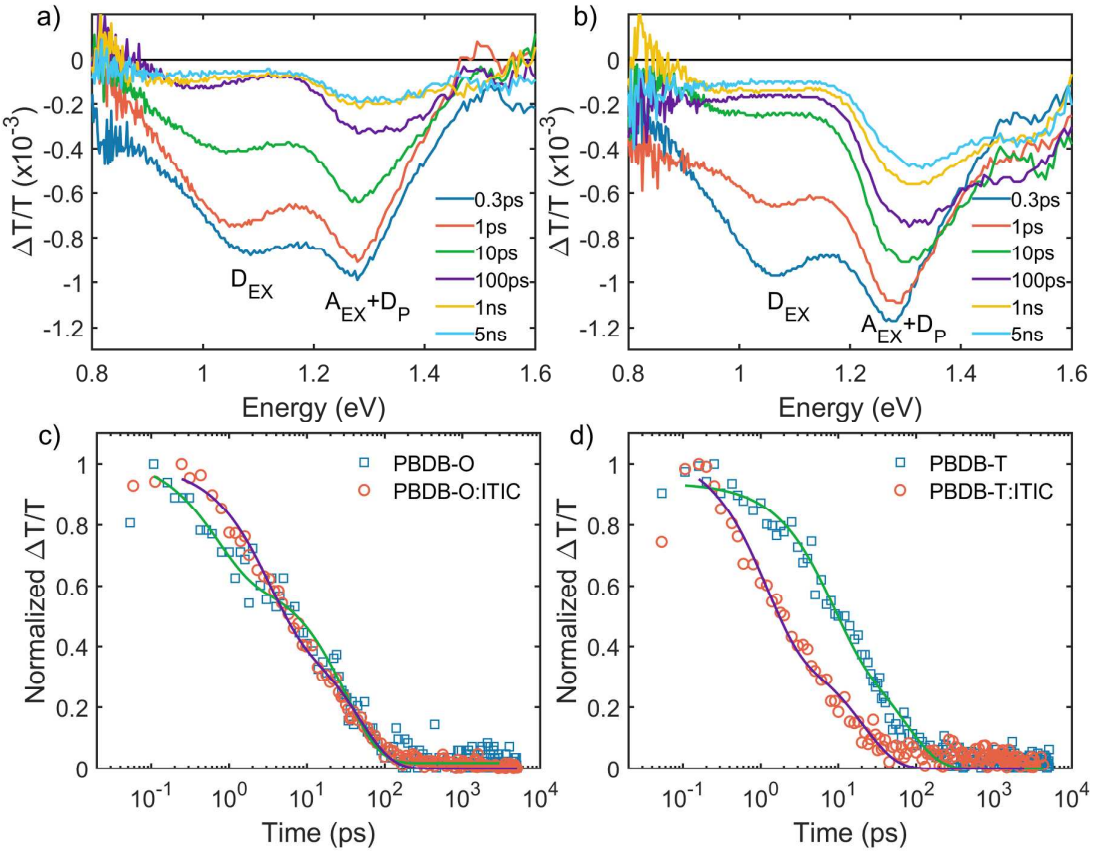

generation is hindered, which might contribute to loss in Jsc.

Figure 2. a and b) Transient absorption spectra in the IR region. Excitation is tuned to 520 nm (2.38 eV) and the probe pulse is at 0.3 ps, 0.5 ps, 1 ps, 10 ps, 50 ps and 1 ns delay times for PBDB-O:ITIC, and PBDB-T:ITIC. c and d) Exciton decay profiles for neat PBDB-O and PBDB-O:ITIC blend, and neat PBDB-T and PBDB-T:ITIC blend.

Table 2: Exciton and polaron lifetimes (from TAS) of the neat and blend films. SCLC mobility results of neat and blend films

Film	Exciton Lifetime (ps)	Hole Mobility ($cm^2 V^{-1} s^{-1}$)	Electron Mobility ($cm^2 V^{-1} s^{-1}$)
PBDB-O	22	1.56×10^{-5}	-
PBDB-O:ITIC	21	3.29×10^{-5}	6.55×10^{-5}
PBDB-T	36	1.04×10^{-4}	-
PBDB-T:ITIC	8	2.32×10^{-4}	2.93×10^{-4}
ITIC	-	-	2.6×10^{-4} [27]

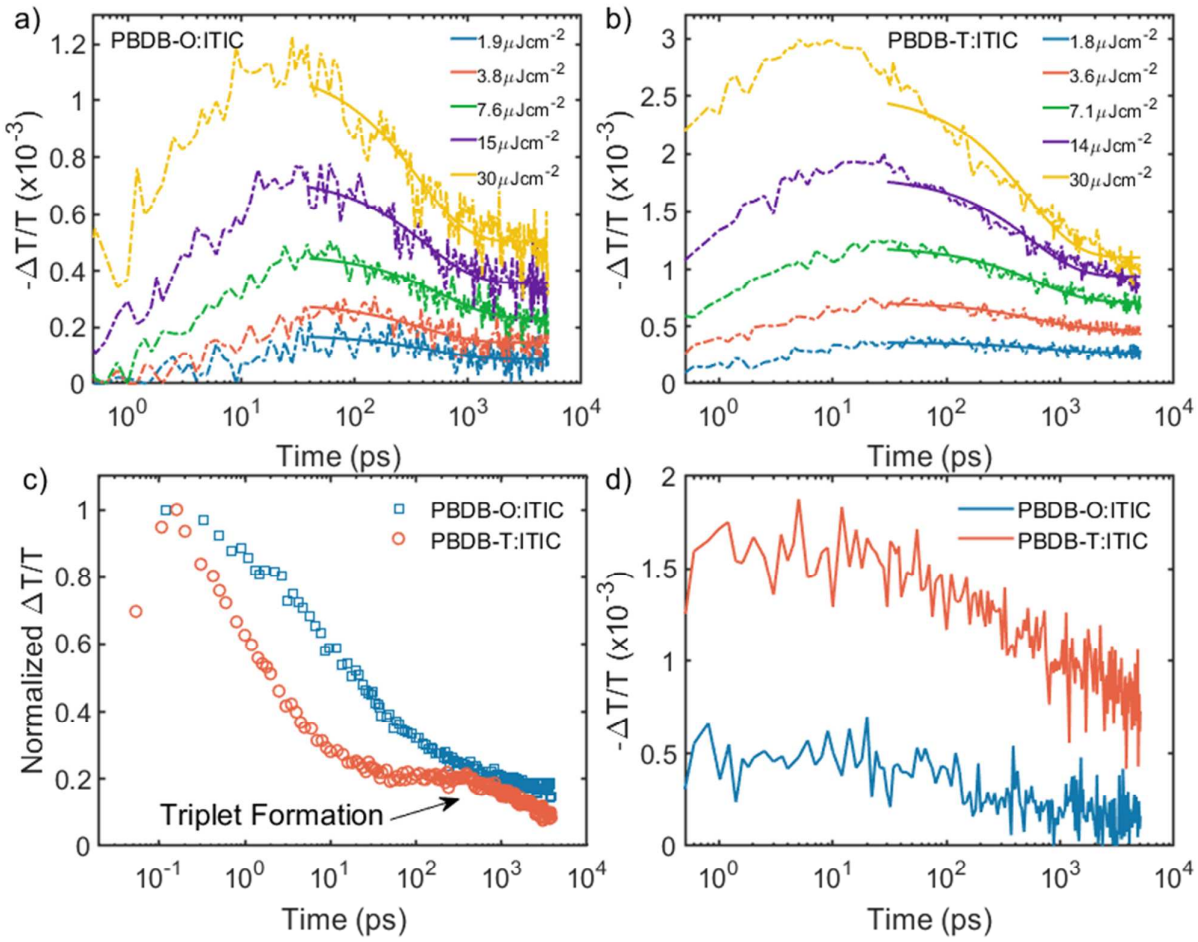

Figure 3. Time evolution of polarons determined from MCR-ALS analysis for the donor excitation (2.28 eV) at the indicated fluences for a) PBDB-O:ITIC, b)PBDB-T:ITIC, c) Comparison of the exciton dynamics of the two blends at the highest fluence (light intensity ~14.28μJ/cm^2), d) Polaron dynamics determined from MCR-ALS analysis for the acceptor excitation (1.77 eV) at a power of 10uW.

We compare the polaron dynamics of both blends at different fluences to study geminate and bimolecular recombination kinetics in the two blends. **Figure 3a and 3b** shows the evolution of the polaron peaks in at different excitation fluences in both blends (see **Figure S4** for normalized fluences). Comparison between the prompt (<500fs) polaron absorption amplitude with the peak polaron absorption amplitude at the lowest fluence of 1.9 μJ/cm^2 indicates that 35% of the total polaron population is formed on ultrafast timescales in PBDB-T:ITIC blend, shown in Figure S1. In stark contrast, PBDB-O:ITIC exhibits almost no ultrafast charge generation. In order to quantify the hole polaron lifetime, the decay of the hole dynamics as shown in Figure 3a and 3b were fit to a the function $N(t) = A_1 e^{-t/\tau_1} + A_2$, where A_1 and A_2 are the proportion of carriers which recombine on sub-nanosecond timescales and those which survive much longer than our experimental time window of 5ns. At the lowest fluence data in **Figure 3a and 3b** the sub-nanosecond recombination yields a time constant of 490 ps for PBDB-O:ITIC and 750 ps for PBDB-T:ITIC. The percentage of carriers which recombine in <1ns is 50% for PBDB-O:ITIC and 26% for PBDB-T:ITIC. Therefore 74% of carriers remain in PBDB-T:ITIC far beyond 5ns as compared to the 50%, which remain in PBDB-O:ITIC. As shown by the fit results in **Table S1** as a function of fluence, the subnanosecond decay rate is highly fluence dependent in PBDB-T:ITIC ranging from 26% of carriers recombine at 750 ps at the lowest fluence to 56% of carriers recombining within 522 ps. In contrast the recombination of polarons in PBDB-O:ITIC is highly fluence independent with roughly 50% of carriers recombine in approximately 500 ps regardless of the excitation fluence. This difference in fluence dependence of recombination dynamics suggest in PBDB-T:ITIC carrier recombine via bimolecular recombination, where as in PBDB-O:ITIC geminate recombination is more dominant. Moreover PBDB-T:ITIC has over three times more polarons generated (see **Table S2**) and and lived for 5ns. This suggests that bimolecular recombination is

dominant in PBDB-T:ITIC blend compared to PBDB-O:ITIC blend. Additional evidence for the strong bimolecular recombination in PBDB-T based blend is the triplet exciton formation during long delay times. **Figure 3c** shows the evolution of the exciton peak in the TAS data in the IR range for very high excitation fluence (14.28 $\mu J/cm^2$). In the PBDB-O:ITIC blend, the exciton peak decays monotonically, whereas in PBDB-T:ITIC the exciton peak at first decays and then grows at later delays. This time delayed growth is a signature of triplet exciton formation due to bimolecular recombination of separated charges. As we performed the TAS experiments in thin-films and no charges are extracted, surviving carriers can bimolecularly recombine and form triplet excitons. Therefore triplet exciton generation is a characteristic signature of bimolecular recombination. The fact that even at high excitation densities triplet excitons do not form at later delays in PBDB-O based blend is a strong indication of geminate recombination or fast recombination of excitons. In contrast, in PDBD-T:ITIC free carriers bimolecularly recombine and form of triplet excitons.[38,39]

In addition, we monitored hole transfer from the electron acceptor ITIC to the donor by measuring the polymer-hole polaron population after selectively exciting the acceptor (E_{ex}= 1.77 eV). In **Figure 3d** the time evolution of the spectral signal that corresponds to the polymer hole polaron feature are shown. The signature of ITIC exciton in the transient absorption spectra and the polymer hole polaron coincides (1.27 eV in **Figure 2a** and **2b** and **Figure S5**).[40] The solid lines in **Figure 3d** shows the time evolution of the 1.27 eV peak for both blends and the neat ITIC sample. The decay of the transient signal for PBDB-O:ITIC and neat ITIC are very similar for the total 5 ns range of the experiment, whereas the PBDB-T blend exhibits a slower decay. This observation suggests that charge separation is more efficient for the PBDB-T blend when the small molecule acceptor is excited.

In order to further probe the contribution of the ITIC to the free charge generation in the blend films, we performed transient absorption measurements in the visible range. In the first set of the experiments an excitation energy of 2.38 eV was used for predominant donor excitation. In the second set of experiments, 1.77 eV pump pulses are used for selective ITIC excitation. **Figure S6** shows the transient absorption spectra of two blends at different delays with predominant donor (Eex=2.38 eV) excitation. In the PBDB-O blends only the ground state bleaching (GSB) signal from the polymer domains is observable. In contrast, in the PBDB-T blend both polymer GSB (energies >1.86 eV) and ITIC GSB (energies<1.86 eV) are observable. The evolution of the spectra at 1.65 eV relates to the electron transfer from polymers to the ITIC in both blends. While in the PBDB-O:ITIC the transient signal at 1.65 eV is very weak (limited by the sensitivity of the instrument), in PBDB-T blend it exhibits a well-pronounced rise during the first 40 ps after excitation (**Figure S7**). When ITIC is selectively excited at 1.77eV, we did not observe a rise in the GSB feature of the PBDB-O polymers **(Figure S8)**. In contrast, in the PBDB-T:ITIC blend, the polymer GSB signal grows for the first 40 ps after ITIC excitation (**Figure S9**). These observations indicate that, unlike the transfer processes in PBDB-O:ITIC, the electron and hole transfer process in PBDB-T:ITIC is efficient and the TAS data in the visible spectral range further supports conclusions of the IR data.

After a comprehensive investigation of the carrier dynamics and recombination mechanisms between the two materials, we want to gain insight into the underlying factors that affect these significantly varying photophysical characteristics, in particular the effect of morphological and structural differences. In order to characterize the impact of the side-chain modification on molecular packing distances, packing order and texture and ultimately device performance, we performed grazing incidence wide-angle X-ray scattering (GIWAXS) on neat and blend films. Several peaks for both PBDB-O:ITIC and PBDB-T:ITIC are observed (see **Figure 4a-c**), but without a strong presence of higher order (h00) peaks in either the IP or OOP directions. This suggests that both blends exhibit high para-crystallinity and/or low overall degree of crystallinity. We do observe that the PBDB-T:ITIC film has a slightly more face-on preferential orientation indicated by the presence of a π-π, i.e. (010) peak in the OOP direction and a (100) peak in the IP direction, a preferential orientation that has often been invoked to explain improved vertical charge transport to the electrodes and increases in Jsc and FF.[13,41] The GIWAXS patterns for the neat films are provided in **Figure S10**. Even though the (010) peak does not have a strong presence in the PBDB-T:ITIC blend film, it does in the neat film at q= 1.72 A^{-1} (see **Figure S10c)**, which is not observed in the PBDB-O film (see **Figure S10b**). This suggests that the neat PBDB-T has a notably more face-on orientation than PBDB-O, which is favorable for a more efficient out-of-plane charge transport. We note that at an incidence angle of 0.12^o (critical angle) high levels of surface ordering are observed in both PBDB-O:ITIC and PBDB-T:ITIC as evidenced by a richer diffraction pattern (**Figure S11)**. Generally, the PBDB-O:ITIC is more ordered at the surface than the PBDB-T:ITIC, indicating improved lamellar ordering at the surface. Overall, both samples have more ordered surfaces than their respective bulks. This is evident as for angles beyond 0.13^o, these sharp features are still present but subdued by the increased contribution less ordered bulks.[42] Moreover, the presence of polymorphs or the presence of a layered structure with unfavorable orientation (edge-on) at one of the interfaces can be contributing factors. This complicates the analysis of the diffraction data, as there is currently no established protocol how to quantify and correlate the various scattering features and precise location of the corresponding structure and texture within the film as a function of depth to performance. The development of such protocols is outside the scope of this comparison.

Generally, the GIWAXS results show some differences between the two blended films that qualitatively supports the better performance of PBDB-T, but we are uncertain how they help explain quantitatively the large difference in performance.

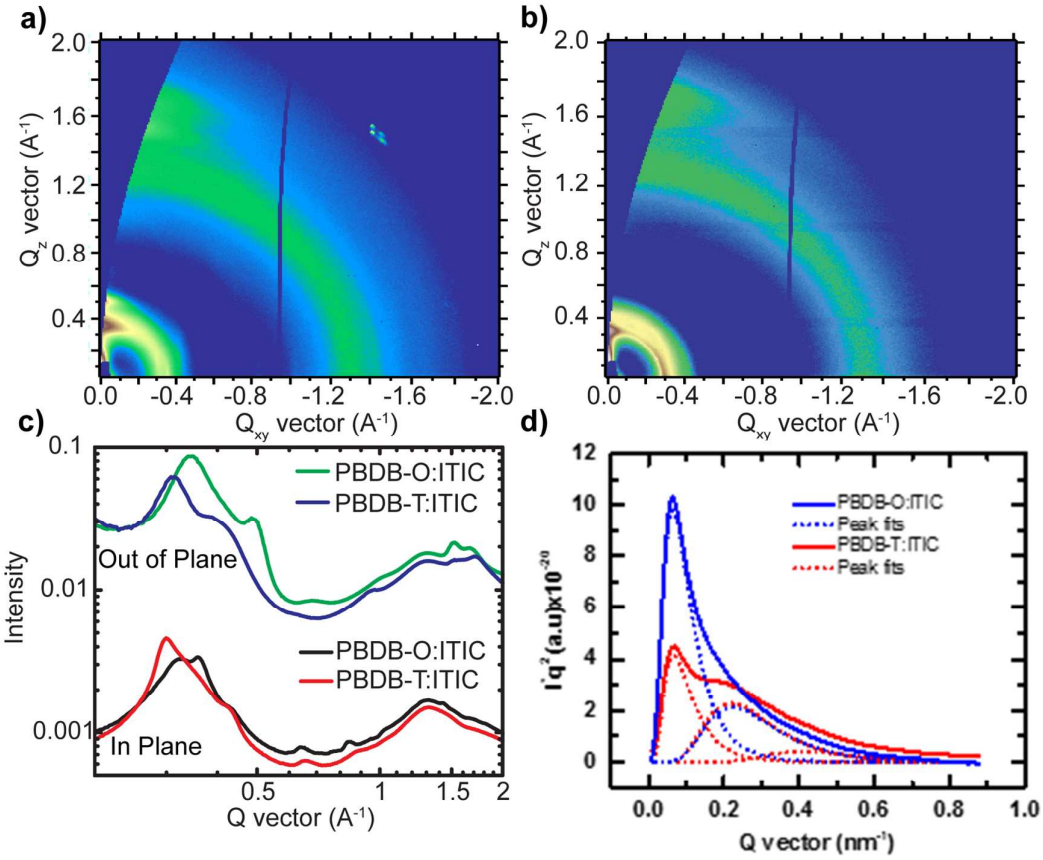

Figure 4. a) and b) show the 2D GIWAXS patterns for PBDB-O:ITIC and PBDB-T:ITIC blend films, respectively. c) Line-cut profiles at incidence angle = 0.15° for PBDB-O:ITIC and PBDB-T:ITIC blend films. d) RSoXS Lorentz-corrected sector averages for PBDB-O:ITIC and PBDB-T:ITIC at a photon energy of 284.2 eV.

We employed Resonant Soft X-ray Scattering (RSoXS) to gain further insight into morphological differences between the chemically similar polymers in the absence of major interpretable differences in molecular packing in the blends. RSoXS probes morphological features on a length scale ranging from 10 to over 500 nm.[43] Thickness normalized Lorentz corrected sector averages for the two blends at a photon energy of 284.2 eV are presented in **Figure 4d**. Such data is akin to the power-spectral density of real space images, measuring the Fourier amplitude of correlations in a sample. The amplitude is proportional to the mean-square variation at a given spatial frequency. It is readily noticeable that both blend films have a peak at q~0.06 nm^{-1}, yet with a significantly larger intensity for the PBDB-O:ITIC film. Moreover, a broad peak/shoulder at a higher q of ~0.22 nm^{-1} is present in the PBDB-T:ITIC that is not readily observed in the PBDB-O:ITIC. In order to quantify these differences, multi-peak fitting was performed to both profiles using lognormal functions (see **Figure S12**). In the PBDB-O:ITIC film, a multi-length scale morphology is discerned with correlations in the composition that would correspond to long periods of 100 and 28 nm. As for the PBDB-T:ITIC morphology, a three peak fit was required for a best fit and correlations correspond to long periods of 95, 29 and 15 nm. The percentage of a peak's area to the total scattering area allows for a quantitative way to estimate the mean-square variations at a specific spatial frequency and thus spacing within the film morphology. Peak 1 in the PBDB-O:ITIC profile comprises more than 65% of the total area of the two peaks. Since domain size can be roughly estimated in a 50:50 blends to be ½ the long periods, we can state that the PBDB-O:ITIC sample predominantly consists of large domains (~50nm). It is important to note that this estimation is an upper limit for the domain size as it assumes pure domains in the samples. In the PBDB-T:ITIC film we observe a ~40% intensity for variations at large length scale (domains ~49 nm), and the remaining 60% intensity correspond to correlations at smaller long periods (domains ~15 and ~8 nm). The presence of a larger mean-square composition variations at small length scale in the highest efficiency system (PBDB-T:ITIC) is in agreement with previous reports that showed positive correlation between the presence of such variations and FF and Jsc.[44] Since the real space information is lost in scattering, visualization of the scattering data is model dependent and the

scattering intensity at the different length scales could either come from a hierarchical morphology or morphology, in which regions of space are characterized by different length scales. In the latter visualization, the scattering intensity would measure the volume fraction of domains with the appropriate spacing. The total scattering intensity and thus the mean-square variations that reflect the average purity of the domains within a 3D isotropic morphology is significantly larger for the PBDB-O:ITIC than for the PBDB-T:ITIC. Higher purity is generally associated with better FF.[18,45,46,47,48] This relationship can break down if the domains get too pure and percolation is lost, leading to islands that act as traps that reduce current with a monomolecular signature. FF is also negatively impacted with loss of percolation, but less so than current.[49,50,51] The impact of loss of percolation has not yet been studied systematically to allow quantitative conclusions, nor do we know here the absolute purity of the domains to definitively implicate loss of percolation as the primary cause of the reduced performance of PBDB-O:ITIC. The multi length-scale morphologies complicates matters further.

When peak-fitting is applied in RSoXS data analysis, log-normal correlation distributions are observed in most cases, including previous experiments on PTB7:PCBM that observed dispersed round domains in real space[52]. It is important to note here that careful language must be used when interpreting RSoXS data, as reciprocal-space log-normal data is being transformed to real-space. During this transformation only the median value of the distribution remains unchanged.[53] While the form factor of the morphology constituents is often unknown, the length of a 1D path of an exciton or charge within the same domain is accurately reflected by the correlation distribution, no matter whether the correlations arises from a form factor or a structure factor. The peak location in the log-normal distribution certainly represents a dominant size or spacing through the measured sample, with the assumption of a domain size distribution. This spacing is referred to as the 'long period'. The comparative studies undertaking here would not change in their conclusions if mean, median, or mode characteristics of the log-normal distribution are used.

Since charge creation and charge extraction have been shown to depend on the local [54,55] as well as the overall device moblility,[56,57] we investigate the electron and hole mobility in the neat and the blend films. Using space charge limited current (SCLC), the device hole mobility for the PBDB-O and PBDB-T neat films, electron mobility of ITIC, as well as the hole and electron mobility of the blends were measured and are summarized in **Table (2)**. With over 600% increase in hole mobility and 300% in electron mobility, PBDB-T:ITIC is able to extract free charges faster out of the device contributing to its higher Jsc and FF.[56,57] These large differences in carrier mobility correlate with the geminate recombination that lowers J_{sc} for the PBDB-O over the PBDB-T based devices.

There are several factors that dictate the electron and hole mobility in an organic semiconductor. With the molecular weight and PDI being similar for both polymers, the main factors are molecular packing, morphological differences, wetting layers, and intrinsic molecular level differences. The minor side-chain modification between these two materials does not appear to have as visible of an impact on morphology as it does on the substantially varying device performance. Nonetheless, RSoXS results show that a large composition variation at small length scales in the PBDB-T:ITIC, on the order of typical exciton diffusion lengths, is likely to facilitate exciton dissociation into free charges by lowering geminate recombination, following argument by Burke and McGehee**.**[55] In addition, it is possible that electro-optical features, not investigated in this study, such as overlap of D:A wavefunctions can have a significant influence on device performance. The photophysical differences explored in this study between the two materials such as exciton and polaron lifetimes as well as dominant recombination mechanisms show that the far superior conversion efficiency of PBDB-T:ITIC is elucidated with a more efficient exciton splitting, longer polaron lifetimes, and an enhanced carrier generation contribution by ITIC. However, the stark difference in hole and electron mobility between these two materials plays, likely, the biggest role in dictating device performance. The hole and electron mobility in PBDB-T:ITIC are enhanced by a factor of 6 and 3, respectively. Not only are the hole and electron mobility enhanced in the PBDB-T:ITIC, but they are also more balanced. This is essential for an improved FF. Higher mobility also improve charge transport and subsequently EQE (Jsc), they play a key factor in charge creation as well. The combined impact of these various factors, in addition to possibly others, allow the photo-conversion process PBDB-T:ITIC to be much more efficient than PBDB-O:ITIC.

4. Conclusions

We investigated two similar materials distinguished by minor side-chain differences, PBDB-O and PBDB-T, which when blended with ITIC yield efficiencies of 4.35% and 11.21%, respectively. In order to elucidate this stark difference in performance between these chemically similar material systems, and what factors played a role in dictating these varying efficiencies, we delineated the various photophysical characteristics between the two materials and their blends. We observed that PBDB-T:ITIC has longer polaron lifetimes (>5000 ps) and reduced geminate recombination. RSoXS results showed that a larger mean-square composition variation at small length scales on the order of typical diffusion lengths in the PBDB-T:ITIC is likely to improve exciton dissociation into free charges by lowering geminate recombination. Lastly and most importantly, the significantly improved as well as more balanced electron and hole mobility in PBDB-T:ITIC contribute to

more efficient charge creation and extraction improving the overall efficiency of the blend. Our characterization of the PBDB-O:ITIC and PBDB-T:ITIC systems shows that the photophysics, the morphology, packing, and most notably carrier mobility can be changed through minor side-chain manipulation of otherwise chemically similar materials, leading to a cumulative drastic change in performance. Additional studies focusing on systematic side-chain manipulation of photovoltaic materials seeking optimal optoelectronic properties, in particular blended with non-fullerene acceptors are needed to achieve rational design strategies that push efficiencies of organic solar cells even higher.

Acknowledgements

O.A. and H.A. are supported by the Office of Naval Research (ONR) grant N00141512322 and UNC-GA Research Opportunity Initiative grant. X-ray data were acquired at beamlines 11.0.1.2 and 7.3.3 and 5.3.2 at the Advanced Light Source, which is supported by the Director, Office of Science, Office of Basic Energy Sciences, of the U.S. Department of Energy under Contract No. DE-AC02-05CH11231. A. Hunt is acknowledged for assisting with the measurements and data acquisition. C. Wang, E. Schaible, and C. Zhu are acknowledged for help with x-ray experimental setup and maintenance of the beamline. Time resolved photoluminescence and transient absorption spectroscopy work at NCSU (B.G and K.G) was supported by ONR grant N000141310526 P00002. J. H and W. Z. acknowledge the financial support from the National Natural Science Foundation of China (Nos. 91333204, 21325419), the Strategic Priority Research Program of the Chinese Academy of Sciences (XDB12030200).

References

1 C. B. Nielsen, S. Holliday, H.-Y. Chen, S. J. Cryer and I. McCulloch, *Acc. Chem. Res.*, 2015, **48**, 2803–12.
2 W. Zhao, D. Qian, S. Zhang, S. Li, O. Inganäs, F. Gao and J. Hou, *Adv. Mater.*, 2016, **28**, 4734-4739.
3 H. Yao, Y. Chen, Y. Qin, R. Yu, Y. Cui, B. Yang, S. Li, K. Zhang and J. Hou, *Adv. Mater.*, 2016, **28**, 8283-8287.
4 Y. Lin, Q. He, F. Zhao, L. Huo, J. Mai, X. Lu, C. J. Su, T. Li, J. Wang, J. Zhu, Y. Sun, C. Wang and X. Zhan, *J. Am. Chem. Soc.*, 2016, **138**, 2973–2976.
5 Y. Lin, Z.-G. Zhang, H. Bai, J. Wang, Y. Yao, Y. Li, D. Zhu and X. Zhan, *Energy Environ. Sci.*, 2015, **8**, 610–616.
6 Y. Lin, P. Cheng, Y. Li and X. Zhan, *Chem. Commun*, 2012, **48**, 4773–4775.
7 J. Liu, S. Chen, D. Qian, B. Gautam, G. Yang, J. Zhao, J. Bergqvist, F. Zhang, W. Ma, H. Ade, O. Inganäs, K. Gundogdu, F. Gao and H. Yan, *Nat. Energy*, 2016, **1**, 16089.
8 R. Shivanna, S. Shoaee, S. Dimitrov, S. K. Kandappa, S. Rajaram, J. R. Durrant and K. S. Narayan, *Energy Environ. Sci.*, 2014, **7**, 435.
9 Y. Fang, A. K. Pandey, A. M. Nardes, N. Kopidakis, P. L. Burn and P. Meredith, *Adv. Energy Mater.*, 2013, **3**, 54–59.
10 J. D. Douglas, M. S. Chen, J. R. Niskala, O. P. Lee, A. T. Yiu, E. P. Young and J. M. J. Fréchet, *Adv. Mater.*, 2014, **26**, 4313–4319.
11 K. R. Graham, C. Cabanetos, J. P. Jahnke, M. N. Idso, A. El Labban, G. O. N. Ndjawa, T. Heumueller, K. Vandewal, A. Salleo, B. F. Chmelka, A. Amassian, P. M. Beaujuge and M. D. McGehee, *J. Am. Chem. Soc.*, 2014, **136**, 9608–9618.
12 W. Ma, J. R. Tumbleston, M. Wang, E. Gann, F. Huang and H. Ade, *Adv. Energy Mater.*, 2013, **3**, 864–872.
13 W. Ma, J. R. Tumbleston, L. Ye, C. Wang, J. Hou and H. Ade, *Adv. Mater.*, 2014, **26**, 4234–4241.
14 N. D. Treat, M. A. Brady, G. Smith, M. F. Toney, E. J. Kramer, C. J. Hawker and M. L. Chabinyc, *Adv. Energy Mater.*, 2011, **1**, 82–89.
15 B. A. Collins, E. Gann, L. Guignard, X. He, C. R. McNeill and H. Ade, *J. Phys. Chem. Lett.*, 2010, **1**, 3160–3166.
16 J. R. Tumbleston, B. A. Collins, L. Yang, A. C. Stuart, E. Gann, W. Ma, W. You and H. Ade, *Nat. Photonics*, 2014, **8**, 385–391.
17 G. O. Ngongang Ndjawa, K. R. Graham, R. Li, S. M. Conron, P. Erwin, K. W. Chou, G. F. Burkhard, K. Zhao, E. T. Hoke, M. E. Thompson, M. D. McGehee and A. Amassian, *Chem. Mater.*, 2015, **27**, 5597–5604.
18 S. Mukherjee, C. M. Proctor, G. C. Bazan, T. Q. Nguyen and H. Ade, *Adv. Energy Mater.*, 2015, **5**, 1500877.
19 S. Mukherjee, C. M. Proctor, J. R. Tumbleston, G. C. Bazan, T. Q. Nguyen and H. Ade, *Adv. Mater.*, 2015, **27**, 1105–1111.
20 H. Bin, L. Gao, Z.-G. Zhang, Y. Yang, Y. Zhang, C. Zhang, S. Chen, L. Xue, C. Yang, M. Xiao and Y. Li, *Nat. Commun.*, 2016, **7**, 13651.
21 L. Ye, W. Jiang, W. Zhao, S. Zhang, D. Qian, Z. Wang and J. Hou, *Small*, 2014, **10**, 4658–4663.
22 M. Stolterfoht, A. Armin, S. Shoaee, I. Kassal, P. Burn and P. Meredith, *Nat. Commun.*, 2016, **7**, 11944.
23 Y. Liu, J. Zhao, Z. Li, C. Mu, W. Ma, H. Hu, K. Jiang, H. Lin, H. Ade and H. Yan, *Nat. Commun.*, 2014, **5,** 5293.
24 L. Ye, X. Jiao, M. Zhou, S. Zhang, H. Yao, W. Zhao, A. Xia, H. Ade and J. Hou, *Adv. Mater.*, 2015, **27**, 6046–6054.

25 L. Yang, J. Tumbleston, H. Zhou, H. Ade and W. You, *Energy Environ. Sci.*, 2013, **6**, 316–326.
26 D. Qian, L. Ye, M. Zhang, Y. Liang, L. Li, Y. Huang, X. Guo, S. Zhang, Z. Tan and J. Hou, *Macromolecules*, 2012, **45**, 9611–9617.
27 Y. Lin, F. Zhao, Q. He, L. Huo, Y. Wu, T. C. Parker, W. Ma, Y. Sun, C. Wang, D. Zhu, A. J. Heeger, S. R. Marder and X. Zhan, *J. Am. Chem. Soc.*, 2016, **138**, 4955–4961.
28 A. Hexemer, W. Bras, J. Glossinger, E. Schaible, E. Gann, R. Kirian, A. MacDowell, M. Church, B. Rude and H. Padmore, *J. Phys. Conf. Ser.*, 2010, **247**, 012007.
29 E. Gann, A. T. Young, B. A. Collins, H. Yan, J. Nasiatka, H. A. Padmore, H. Ade, A. Hexemer and C. Wang, *Rev. Sci. Instrum.*, 2012, **83**, 45110.
30 S. D. Dimitrov, B. C. Schroeder, C. B. Nielsen, H. Bronstein, Z. Fei, I. McCulloch, M. Heeney, J. R. Durrant, *Polymers* 2016, **8**, 14.
31 B. R. Gautam, R. Younts, W. Li, L. Yan, E. Danilov, E. Klump, I. Constantinou, F. So, W. You, H. Ade and K. Gundogdu, *Adv. Energy Mater.*, 2016, **6**, 1501032.
32 A. C. Jakowetz, M. L. Böhm, J. Zhang, A. Sadhanala, A. A. Bakulin, A. Rao and R. H. Friend, *J. Am. Chem. Soc.*, 2016, **138,** 11672–11679.
33 B. R. Gautam, C. Lee, R. Younts, W. Lee, E. Danilov, B. J. Kim and K. Gundogdu, *ACS Appl. Mater. Interfaces*, 2015, **7**, 27586–27591.
34 K. Kawashima, Y. Tamai, H. Ohkita, I. Osaka and K. Takimiya, *Nat. Commun.*, 2015, **6**, 10085.
35 R. Shivanna, S. Shoaee, S. Dimitrov, S.K. Kandappa, S. Rajaram, J.R. Durrant, K. Narayan, *Energy & Environ. Sci.,* 2014, **7**, 435-441.
36 Etzold, I.A. Howard, N. Forler, A. Melnyk, D. Andrienko, M.R. Hansen, F. Laquai, *Energy Environ. Sci.* 2015, **8**, 1511-1522.
37 T. Kim, R. Younts, W. Lee, S. Lee, K. Gundogdu, B.J. Kim, *J. Mater. Chem. A*, 2017, **5**, 22170-22179.
38 P.C. Chow, S. Gélinas, A. Rao, R.H. Friend, *J. Am. Chem. Soc.,* 2014, **136**, 3424–3429.
39 D.W. Gehrig, I.A. Howard, F. Laquai, *J. Phys. Chem. C,* 2015, **119**, 13509–13515.
40 Z. Zheng, O.M. Awartani, B. Gautam, D. Liu, Y. Qin, W. Li, A. Bataller, K. Gundogdu, H. Ade, J. Hou, *Adv. Mater.*, 2017, **29**, 1604241.
41 W. Li, S. Albrecht, L. Yang, S. Roland, J. R. Tumbleston, T. McAfee, L. Yan, M. A. Kelly, H. Ade, D. Neher and W. You, *J. Am. Chem. Soc.*, 2014, **136**, 15566–15576.
42 L. A. Perez, P. Zalar, L. Ying, K. Schmidt, M. F. Toney, T. Q. Nguyen, G. C. Bazan and E. J. Kramer, *Macromolecules*, 2014, **47**, 1403–1410.
43 J. H. Carpenter, A. Hunt and H. Ade, *J. Electron Spectros. Relat. Phenomena*, 2015, **200,** 2–14.
44 B. A. Collins, Z. Li, J. R. Tumbleston, E. Gann, C. R. McNeill and H. Ade, *Adv. Energy Mater.*, 2013, **3**, 65–74.
45 X. Jiao, L. Ye and H. Ade, *Adv. Energy Mater.*, 2017, **7**, 1700084.
46 L. Ye, X. Jiao, S. Zhang, H. Yao, Y. Qin, H. Ade and J. Hou, *Adv. Energy Mater.*, 2017, **7**, 1601138.
47 A. C. Stuart, J. R. Tumbleston, H. Zhou, W. Li, S. Liu, H. Ade and W. You, *J. Am. Chem. Soc.*, 2013, **135**, 1806–1815.
48 L. Ye, H. Hu, M. Ghasemi, T. Wang, B. A. Collins, J-H. Kim, K. Jiang, J. Carpenter, H. Li, Z. Li, T. McAfee, J. Zhao, X. Chen, J. Y. L. Lai, T. Ma, J-L. Bredas, H. Yan, and H. Ade, *Nat. Mater.*, 2017, in press.
49 J. A. Bartelt, Z. M. Beiley, E. T. Hoke, W. R. Mateker, J. D. Douglas, B. A. Collins, J. R. Tumbleston, K. R. Graham, A. Amassian, H. Ade, J. M. J. Fréchet, M. F. Toney and M. D. Mcgehee, *Adv. Energy Mater.*, 2013, **3**, 364–374.
50 N. Li, J. D. Perea, T. Kassar, M. Richter, T. Heumueller, G. J. Matt, Y. Hou, N. S. Güldal, H. Chen, S. Chen, S. Langner, M. Berlinghof, T. Unruh and C. J. Brabec, *Nat. Commun.*, 2017, **8**, 14541.
51 L. Ye, B. A. Collins, X. Jiao, J. Zhao, H. Yan, and H. Ade, *Adv. Energy Mater.,* 2017. doi:10.1002/aenm.201703058..
52 B.A. Collins, Z. Li, J.R. Tumbleston, E. Gann, C.R. McNeill, H. Ade, *Adv. Energy Mater*., 2013, **3**, 65-74.
53 J.H. Carpenter, A. Hunt, H. Ade, *J. Electron. Spectrosc. Relat. Phenom.*, 2015, **200**, 2-14.
54 S. Gélinas, A. Rao, A. Kumar, S. L. Smith, A. W. Chin, J. Clark, T. S. van der Poll, G. C. Bazan and R. H. Friend, *Science,* 2014, **343**, 512–516.
55 T. M. Burke and M. D. McGehee, Adv. Mater., 2014, **26**, 1923–1928.
56 D. Bartesaghi, I. D. C. Pérez, J. Kniepert, S. Roland, M. Turbiez, D. Neher and L. J. A. Koster, *Nat. Commun.*, 2015, **6**, 7083.
57 U. Würfel, D. Neher, A. Spies and S. Albrecht, *Nat. Commun.*, 2015, **6**, 6951.